scientific reports

Check for updates

OPEN

Controlled tumor heterogeneity in a co-culture system by 3D bio-printed tumor-on-chip model

Nafiseh Moghimi[1,2]✉, Seied Ali Hosseini[3], Altay Burak Dalan[1,4], Dorsa Mohammadrezaei[1], Aaron Goldman[2,5] & Mohammad Kohandel[1]

Cancer treatment resistance is a caused by presence of various types of cells and heterogeneity within the tumor. Tumor cell–cell and cell-microenvironment interactions play a significant role in the tumor progression and invasion, which have important implications for diagnosis, and resistance to chemotherapy. In this study, we develop 3D bioprinted in vitro models of the breast cancer tumor microenvironment made of co-cultured cells distributed in a hydrogel matrix with controlled architecture to model tumor heterogeneity. We hypothesize that the tumor could be represented by a cancer cell-laden co-culture hydrogel construct, whereas its microenvironment can be modeled in a microfluidic chip capable of producing a chemical gradient. Breast cancer cells (MCF7 and MDA-MB-231) and non-tumorigenic mammary epithelial cells (MCF10A) were embedded in the alginate-gelatine hydrogels and printed using a multi-cartridge extrusion bioprinter. Our approach allows for precise control over position and arrangements of cells in a co-culture system, enabling the design of various tumor architectures. We created samples with two different types of cells at specific initial locations, where the density of each cell type was carefully controlled. The cells were either randomly mixed or positioned in sequential layers to create cellular heterogeneity. To study cell migration toward chemoattractant, we developed a chemical microenvironment in a chamber with a gradual chemical gradient. As a proof of concept, we studied different migration patterns of MDA-MB-231 cells toward the epithelial growth factor gradient in presence of MCF10A cells in different ratios using this device. Our approach involves the integration of 3D bioprinting and microfluidic devices to create diverse tumor architectures that are representative of those found in various patients. This provides an excellent tool for studying the behavior of cancer cells with high spatial and temporal resolution.

Abbreviations

TME	Tumor microenvironment
2D	Two-dimensional
3D	Three-dimensional
ECM	Extracellular matrix
EGF	Epithelial growth factor
DMSO	Dimethyl sulfoxide
DMEM	Dulbecco's modified Eagle's medium
MTT	3-(4,5-Dimethyl-2-thiazol)-2,5-diphenyl-2H-tetrazolium bromide
FBS	Fetal bovine serum

Breast cancer is the most common cancer in women and the second most common cancer overall[1]. There were over two million new cases in 2018, and more than 30% of those women died[1]. The aggressiveness of breast cancer may be due to the known heterogeneity of breast tumors[2]. Tumor heterogeneity has been observed among patients (inter-tumor heterogeneity) and in each individual tumor (intratumor heterogeneity), which leads to breast cancer aggressiveness and challenges in treatment[3]. Since tumor may consist of phenotypically different cancer cell populations with different properties, tumor specimen obtained by biopsy does not represent the exact

[1]Department of Applied Mathematics, University of Waterloo, Waterloo, Canada. [2]Department of Medicine, Harvard Medical School, Boston, MA, USA. [3]Electrical Engineering Department, University of Waterloo, Waterloo, Canada. [4]Department of Medical Genetics, School of Medicine, Yeditepe University, Istanbul, Turkey. [5]Division of Engineering in Medicine, Brigham and Women's Hospital, Boston, MA, USA. ✉email: nmoghimi@uwaterloo.ca

tumor composition. In the case of intratumor heterogeneity, the tumor consists of different phenotypical cell populations, which can be identified by different cell phenotypes, cell density, or their localization in the tumor[4,5].

Conventional models lack spatial cellular heterogeneity of breast cancer and usually depend on external stimuli or stresses which make them challenging in the formation and study of physiological tumors[6]. Two-dimensional (2D) culture models also cannot mimic the tumor heterogeneity and microenvironment[7], while tumour growth in vivo occurs in a three-dimensional (3D) environment in which the cancer cells are in constant and intimate contact with the extracellular matrix (ECM) and other cells. 3D cancer models development provides economic and ethical benefits for the prediction of tumor response to treatment by reproducing important aspects of tumors, such as the presence of oxygen and nutrients gradients, cell–cell interactions, drug penetration and subpopulations of quiescent cells[8]. Furthermore, 3D in vitro models are bridging the gap between 2D and in vivo studies, thereby reducing the number of animals sacrificed in preclinical studies[9]. By adding a microfluidic system to a 3D culture in a so-called tumor-on-chip system, recapitulation of the TME gets even more accurate, providing valuable insights into cancer biology[10,11].

Microfluidic platforms are being used for in vitro studies to mimic physical and chemical stimuli in cell migration including enviromental stiffness[12]. They also used to investigate cancer extravasation by transmission across an endothelial monolayer[13], perfusable bone-mimicking microenvironment[14], or through a micro-vascular network[15,16]. However, these devices show some limitations, due to over-miniaturization, poor cells number and mostly model in 2D fashion. Beside tumor-on-chip models, other in vitro models are developed to investigate cell migration and metastasis mechanism including anti-metastatic agents. Knowing the crosstalk role between cancer cells and host cells in the metastatic cascade, multilayered models developed that can mimic relatively similar in vivo microenvironment[17,18]. Transwell systems are also used (with and without hydrogel) where a particular cell type is seeded over a porous membrane and another on the bottom of a culture plate[19,20].

Bioprinting recently attracted much attention because of its ability to build tissue constructs by precise positioning of cells and biomaterials in a layer-by-layer procedure[21,22]. In this method, living cells and ECM components are printed together, making a 'bioink', which can recapitulate the compositional and geometric complexity of the tumor microenvironment (TME) while preserving cell viability[23–25]. Current bioprinting methods include inkjet, extrusion, and laser-assisted printing[26,27]. Among them, the extrusion method features versatile material selections and allows tumor heterogeneity to be controlled within the printed matrices by tight spatial control of distinct types of materials at different initial locations[27]. This highly reproducible process also enables the deposition of materials that have cells of a known density embedded in them. The main advantage of extrusion bioprinting technology is the ability to deposit very high cell densities close to physiological cell densities, which is a major goal of bioprinting methods[26,27]. Extrusion bioprinting has been successfully used to build human-scale tissue construct[28], vascular structures[29,30] and skin tissues[31,32], and results in high printing fidelity and cell viability.

Our goal is to establish a platform for modeling the phenotypic heterogeneity that can occur due to different cell localization in a tumor (tumor center or periphery, uneven oxygen amount) and/or interaction with TME. The present work covers the design and construction of in vitro tumor models via physical and chemical means by the 3D bioprinting of co-cultured cells with controlled distribution in a hydrogel matrix in a microfluidic device. Our hypothesis is that the tumor could be represented by a cancer cell-laden co-culture hydrogel construct, whereas its microenvironment can be modeled in a microfluidic chip capable of producing a chemical gradient. Our composite hydrogel as a bioink comprised of alginate and gelatin, which is compatible to the microscopic architecture of a native tumor stroma. The cell-laden structures which are breast cancer cells embedded in the hydrogels and printed via an extrusion-based bioprinter will create a 3D model tumor that mimics the in vivo microenvironment. We have optimized our bioink based on printability and cell viability measurements. Co-cultured 3D bioprinted constructs are developed with the best chosen bioink. We use a multi-cartridge extrusion bioprinter that allows us to develop cellularly heterogeneous samples comprised of two different breast cancer cells in specific initial locations, specific architecture with controlled density.

Engineering a migration-inducing chemical microenvironment is employed for the creation of an in vitro platform to address metastatic behaviour, which has not yet been fully achieved by current in vitro tumor models. Extracellular chemical gradients are dynamically manipulated via 3D printed constructs containing growth factors in the chamber, enabling post-print cellular modulation. This approach allows for both spatial (via the 3D printing) and temporal (via the gradient concentration and flow rate) generation of chemical cues in 3D matrices, plus the dynamic regulation of cellular behaviors at a local level. Epithelial growth factor (EGF) is being used, as a proof of concept, to model the migration of cells in the 3D construct toward the chemoattractant. MDA-MB-231 cells show a different pattern of migration toward the epithelial growth factor gradient in the device when the tumor architecture is different. There are few recent works using organ-on-a-chip platforms to study heterogeneity, or metastasis, in breast cancer[33,34]. However to the best of our knowledge, no studies have been reported on 3D bioprinting of co-cultures in a microfluidic environment with controlled architecture. Furthermore, most of the current in vitro models are either 2D modeling or composed of only one type of cell, while to be physiologically relevant, the model should also address the complex cellular interactions within the TME. Combining these 3D bioprinting approaches for in vitro tumor modeling, with microfluidic devices to model microenvironment, provides tools to create complex tumor architecture accompanied by controlled chemical densities, with a high spatiotemporal resolution, beyond what is possible with conventional fabrication technologies.

Experimental

Materials. Gelatin from bovine skin (type B) and alginic acid sodium salt, dimethyl sulfoxide (DMSO), calcium chloride, and sodium chloride powder were purchased from Sigma-Aldrich (Canada). Calcium chloride was dissolved in Millipore water at a final concentration of 4%, filtered with 0.2 u filters and stored in a

sterile condition for further use. For cell culture studies, MCF7 and MDA-MB-231 cell lines were purchased from ATCC (Cedarlane, Canada). DMEM (Dulbecco's Modified Eagle's Medium, without sodium pyruvate, with 4.5 g/l glucose, with L-glutamine), PBS (phosphate buffer saline) 1×, Penicillin-streptomycin, Trypsin/EDTA solution at 0.25% (w./v.) and FBS (fetal bovine serum) were purchased from Wisent Bioproducts (Canada). (3-(4,5-dimethyl-2-thiazol)-2,5-diphenyl-2H-tetrazolium bromide) MTT powder, Triton X-100, BSA (bovine serum albumin), paraformaldehyde, a Live/Dead Cell Viability assay kit (CBA415) and Hoechst 33342 Nuclei Dye, Propidium Iodide (PI) and Calcine were bought from Sigma-Aldrich (Canada). For bioprinting, the mixing syringe (5ml) with the mixing ratio of 4:1, and compatible mixer tips were purchased from Sulzer Inc. (Switzerland). Empty cartridges and nozzles purchased from Cellink (Sweden)

Preparation of bioink. Sodium alginate and gelatin (type A, 90–110 bloom derived from porcine skin) were purchased from Sigma Aldrich (St. Louis, MO). Bioink formulations were prepared with various ratios of alginate and gelatin. According to the protocol provided by Ouyang et al.[35] gelatin and alginate powder mixtures with different ratios were first dissolved in 0.5% sodium chloride salt solution. Then the solution was stirred vigorously on a hot plate at 85 °C for half an hour. The hydrogels were moved under a biosafety cabinet and treated with UV light for 20 minutes. Afterward, all bioink formations were kept at room temperature (23–24 °C) for 2–4 h prior to rheological tests and kept in a fridge (4 °C) for longer storage. All subsequent experiments were conducted at room temperature.

We used two types of cells for our experiments: MCF7 and MDA-MB-231 breast cancer cell lines purchased from ATCC. The cells were passaged once or twice a week and cultured in Dulbecco's Modified Eagle's Medium (DMEM) with 10% fetal bovine serum (FBS) and 1% penicillin-streptomycin, called complete DMEM afterward, as recommended by the supplier. Experiments were performed with cells passaged less than ten times. Mixing cells and hydrogel was performed under biosafety cabinet with the dual mixing syringes with the ratio of 4:1 (gel: cell). Cartridges of bioinks containing cells were immediately used for bioprinting under sterile conditions.

Bioprinting process. CELLINK INCREDIBLE+ (CELLINK AB) was used for the printing of single cell and multiple cell laden constructs. The bioinks were loaded into sterile printing cartridges, and the bioink was extruded through nozzles using extrusion-based print-heads. For sequential printing of two different cells, two separate cartridges have been used. The material flow for each print-head was controlled by individual pressure and speed regulators. The moving speed of the needle was adjusted at 5 mms^{-1}. Predefined structures were implemented using Solidworks software and sliced in sli3r software to 10 layers with a rectilinear filling pattern (Fig. 1A). The printability of alginate-gelatin hydrogels, using a combination of different hydrogel compositions and printing pressures, was evaluated (Supplementary Table 1, Supporting Information) using a sterile high precision 22G conical nozzle (0.41 mm inner diameter). All bioink preparation components were sterilised prior to printing by using the UV in BSC and soaking in ethanol 70% for 1 h. Alginate and gelatin powders sterilized under BSC UV for 20 min. Sterilized water is added to the powder and the container is covered. Then the container is put on hot plate for 1 h at 85 °C with magnetic stirring. The prepared ink put under BSC UV light until cool down before mixing with cells. The printer, print bed and print-head were kept at room temperature. The bioprinted constructs were subsequently submerged in 4% (w/v) sterile $CaCl_2$ for 10 min for crosslinking sodium alginate with calcium ions. After 10 minutes, cell-laden constructs were washed three times with PBS, submerged in a growth medium (DMEM) containing 10% FBS and 1% penicillin/streptomycin and incubated (37 °C, 5% CO_2) for further analysis. The culture medium was exchanged every other day.

Cell viability and proliferation. Cell viability was evaluated, by MTT and live and dead Assays, on bioprinted structures immediately after printing and after 4, 7 and 11 days. Cell viability properties of constructs were determined using a Live/Dead staining viability kit based on the manufacturer's instructions. Briefly, each construct was submerged in 1 µM Calcine-AM dye solution and incubated for 1 h at 37 °C. Then the solution aspirates and the constructs were submerged in 2 µM propidium iodide solution and kept in the dark at room temperature for 30 min. The staining solution was removed, and the constructs were soaked in PBS for 15 min twice. A laser scanning confocal microscope (Zeiss LSM 700) was used to image live and dead cells in the constructs at five technical replicates. Three constructs (three biological replicates) (n = 3) were used to analyze quantitative cell viability. Based on the live and dead images, the quantitative viabilities of cells were manually counted using ImageJ software (NIH) and calculated based on the number of live cells (green stained cells) over the total number of cells (Live + dead).

Cell proliferation within the 3D network of three biological replicates was assayed using MTT assay. 900 µl of DMEM and 100 µl of MTT working solution (0.5 mg mL^{-1} in PBS) were added to each well of a 12-well plate on each construct and incubated for 3 h at 37 °C, 5% CO_2. At the scheduled timing, the medium was discarded, and cells were washed twice with PBS. Cell membranes and insoluble formazan crystals were dissolved by using 1 ml of dimethyl sulfoxide (DMSO) to each structure for 30 min, protected from light. The obtained solution was transferred in a 96-multiwell, and optical density was evaluated at 540 nm using Absorbance Microplate Reader (Biotek Synergy H1, Agilent). Results of cellular viability were expressed as UV–Vis absorbance of each sample compared with the negative control absorbance, which is a 3D construct prototype without cells to exclude the polymer interference in the UV–Vis reading.

Cell staining. The PKH67 and PKH26 Fluorescent Cell Linker Kits were used employing proprietary membrane labeling technology to stably incorporate a green and red fluorescent dye with long aliphatic tails into lipid regions of the cell membrane[36]. Diluent C is used as the labeling vehicle to maintain cell viability while maximizing dye solubility and staining efficiency during the labeling step. The cells were centrifuged and suspended in a

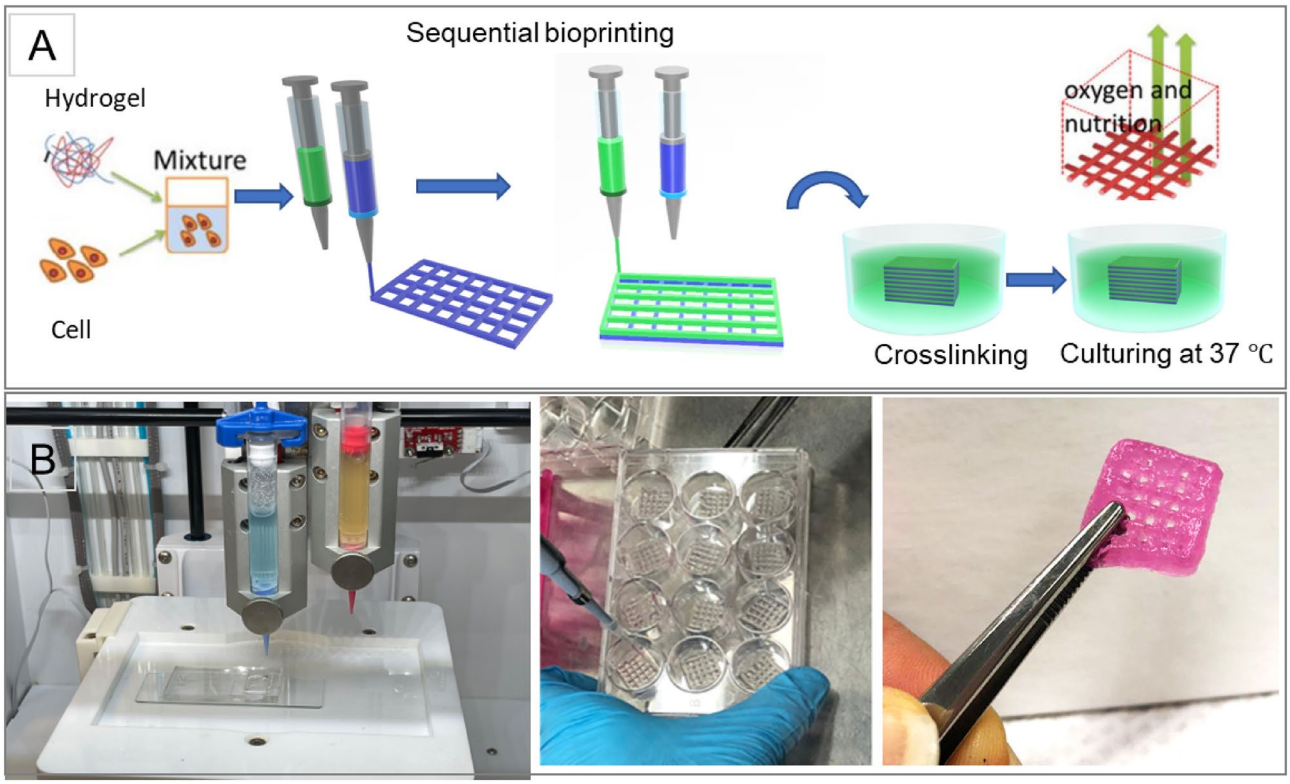

Figure 1. (**A**) The schematic illustration of the biofabrication process, (**B**) the printer and bioprinted constructs (Food coloring used for the purpose of illustration).

medium without serum (DMEM only). 4 µL of the PKH67 (green) or PKH26 (red) was added to 1 mL Diluent C and mixed well to disperse. The cell pellets were dispersed in 1 mL of Diluent C. Rapidly, the cell suspension solution and the dye solution were mixed and homogenized by gentle pipetting and incubated at 37 °C for 5 min. The staining was stopped by adding 10 mL of complete media (DMEM + 10% FBS and 1% penicillin-streptomycin). Cells were centrifuged and washed with DMEM only two more times to ensure the removal of unbound dye.

Microscopic examinations. All constructs were examined for bright field imaging and fluorescent imaging microscope using Nikon Eclipse Ti2 by appropriate filters. A laser scanning confocal microscope (Zeiss LSM 700) was used to observe cell morphology and cell distribution within the 3D printed constructs. At each observation position, a Z-stack scan (400 µm thickness) was implemented with 5 or 10 µm steps at magnifications of ×4.

Rheological measurements. Rheological measurements of bioink formulations were performed with a Malvern Kinexus Ultra$^+$ rheometer with a 20 mm parallel plate geometry with a 1 mm gap. To load the hydrogel sample, the hydrogel was placed on the lower plate of the rheometer, and the steel plate geometry was lowered until contact was established with the surface of the bioink sample. Subsequently, the excess sample around the plate was removed with a spatula. The elastic and viscous moduli of hydrogels were evaluated at 25 °C and 15 °C at a strain of 0.1%. Viscosities of all samples were measured at 25 °C at a shear rate of 1–100 s^{-1}. The shear elastic modulus G', shear loss modulus G'', and loss tangent tan(δ) were measured for each hydrogel bioink using a shear strain sweep test ranging from 0.02 to 1.0% at an oscillation frequency of 40 Hz. All rheological measurements were conducted in triplicate.

Microfluidic chip design and manufacturing. *Design* A tree-like gradient generator is designed that can be integrated with the 3D bioprinting for the tumor-on-chip model. The device contains two inlets for the injection of the culture media as well as the reagent of interest. A linear gradient of the reagent will be produced across a chamber while the waste materials leave the device through six outlets next to this chamber. An algorithm was utilized to find the length of branches in each step of mixing channels, assuming the width of channels and their height were 400 µm and 50 µm respectively. The whole model is 21 mm in width and 45 mm in length.

Fabrication A standard lithography procedure was followed to fabricate a microfluidic gradient generator. Briefly, a 50 µm thick layer of SU8-2050 negative photoresist was spun on a cleaned Si wafer and then was patterned and developed by rinsing in SU8 etchant to form the mold for the microchannels. Next, a 10:1 ratio of PDMS was spread onto the mold and was left for 12 h at 65 °C to completely polymerize. The cast chip in PDMS was peeled off, and holes were punched in the location of the in/outlets. The chamber area was also cut

out using a blade to open some space for the tumor printing. Then, the PDMS layer was bonded to a glass slide using oxygen plasma in plasma cleaner. The as-prepared microfluidic chip was exposed to UV light for disinfection before bioprinting tumors directly in the chamber or transferred to the chamber. Another glass slide was activated using oxygen plasma and sealed the top of the chamber. A flow of cell culture media using a syringe pump was immediately introduced through the inlets to provide cell viability. The source in one of the inlets was then switched with the reagent of interest to form the gradient in the chamber. The device was kept inside an incubator at 37 °C and 5% CO_2 during the whole experiment and was periodically examined.

Tumor-on-chip modeling. Three cell culture models were built in this study, including a 2D model, a sequential 3D bioprinting model and a co-cultured 3D bioprinting, all in on the microfluidic device. The 2D model was prepared simply by culturing MCF7 and MDA-MB-231 cells in 12-well plates to 80% confluency unless otherwise stated. For co-culture experiments, the cells were labelled with different florescent markers before culturing to distinct visibility by fluorescent microscope during the experiment. For sequential bioprinting, a G-code has been prepared for the bioprinter to allow switching between two printheads in alternative layers in which each layer was printed with one of the bioinks including type A or type B cells. For the mixed cell bioprinted constructs, two different cell types were labelled either with green or red markers to be distinguishable. The hydrogel was mixed with cells with the desired ratio of two cells and desired ratio of gel to cells. One cartridge of mixed cells was prepared and printed in a layer-by-layer fashion. For the microfluidic chip experiments, the constructs either be printed directly in the microfluidic chamber or transferred to the chamber later, based on the designed test.

Results

Printability and mechanical properties of bioink. In the preliminary study, various hydrogels with alginate 1–10% and gelatin 4–10% were prepared and printed at room temperature using INKREDIBLE bioprinter (Cellink, Sweden). The small nozzle diameter results in higher resolution, but increases cellular damage because of high extrusion pressure. On the other hand, previous studies reported that low shape fidelity obtained with higher nozzle diameter with low pressure printing[26]. However it provides a better condition for cell viability. A quantitative relationship between nozzle size and dispensing pressure on cell viability has been found[37]. Here, each hydrogel was printed with two nozzle diameters, 25 G (Red, 250 μm inner diameter) 22G (Blue, 410 μm inner diameter). Figure 1A shows the schematic illustration of the biofabrication process and printed structures and Fig. 1B shoes the printed constructs. We continued bioprinting with 22G nozzle that needs less extrusion pressure and was found favorable for cell viability after printing. After making bioink by mixing hydrogel and the cells, the bioprinting procedure was applied sequentially by two print heads containing either cells of type A and cells of type B, separately. Then the printed construct was submerged in $CaCl_2$ for crosslinking for 10 min. After washing by PBS, each construct was immersed in cell media (DMEM, with 10% PBS, 1% Pen-Stripe) and incubated in 37 °C. Supplementary Table 1 (Supporting Information) summarizes the applied pressure, filament condition and quality of the printed structure based on nozzle size and hydrogel composition.

Cell viability. To visualize the distribution of cells in printed construct, cell membranes were pre-stained with a green fluorescent membrane marker (PKH67) before printing and imaged immediately after printing with a confocal microscope. Figure 2A shows that cells were distributed homogeneously in the construct. The viability of different cells after printing was determined using a live-dead staining assay. The live/dead staining reagents were added to each structure immediately after bioprinting, as described in the experimental section. The status of cell survival was defined as the percentage ratio of the live cells over the total cells, where calcium-acetoxymethyl green fluorescence stained live cells and propidium iodide red fluorescence stained dead cells. Cell viability is an essential factor for the successful fabrication of cell-printed constructs. The live-dead assay results (Fig. 2B) show the percentage of viable MDA-MB-231 cells immediately after printing were 94.16%, 96.94%, 75.96%, and 84.7% for hydrogels A1G4, A4G4, A8G4 and, A1G8 respectively. The representing image related to A4G4 with green shows live cells and red indicates dead cells presented in Fig. 2C. The 3D z-stack is shown in Fig. 2D, confirming the homogeneity of live cells in the construct.

3-(4,5-Dimethylthiazol-2-yl)-2,5-diphenyltetrazolium bromide (MTT) assay was conducted on three replicates of 3D bioprinted constructs immediately after printing and after incubation at 37 °C, 5% CO_2 in DMEM with 10% FBS and 1% Penicillin- streptomycin for 4, 7 and 11 days. Results of MTT test are reported in Fig. 2E as absorbance data detected at 570 nm. The data refer to three replicates of 3D bioprinted constructs and three replicates of negative control constructs (small bars) that are 3D printed structures without cells. A clearly good cell distribution into construct can be observed with absorbance values were ~ 0.86 ± 0.02 immediately after printing. An increment of absorbance was measured after incubation for 4 days (1.39 ± 0.05) and continued to reach 1.94 ± 0.04 on day 7. The rate of viability, compared to day 1, increased over the week but on the day 11, the absorbance was 2.07 ± 0.06, which shows a drop in the rate of cell proliferation. It seems that between day 7 to day 11 the constructs reach the maximum capacity for hosting cells and later on some cells started to die.

3D Bioprinted co-cultures. MCF7 cancer cells (a breast adenocarcinoma cell line) and MDA-MB-231 (a more aggressive triple negative breast cancer cell line with mesenchymal characteristics) are pre-stained with green and red markers before printing, respectively. In the first printing procedure, two bioinks were prepared separately from each type of cell and printed sequentially. The first layer of the printed structure consisted of MDA-MB-231 cells (stained red), and the second layer of MCF7 cells (stained green) lay on top of the first layer. In the second printing experiment, one bioink was prepared with both pre-stained cells mixture in the hydrogel and bioprinting was conducted layer-by-layer same as before. Figure 3A,B show the confocal image of

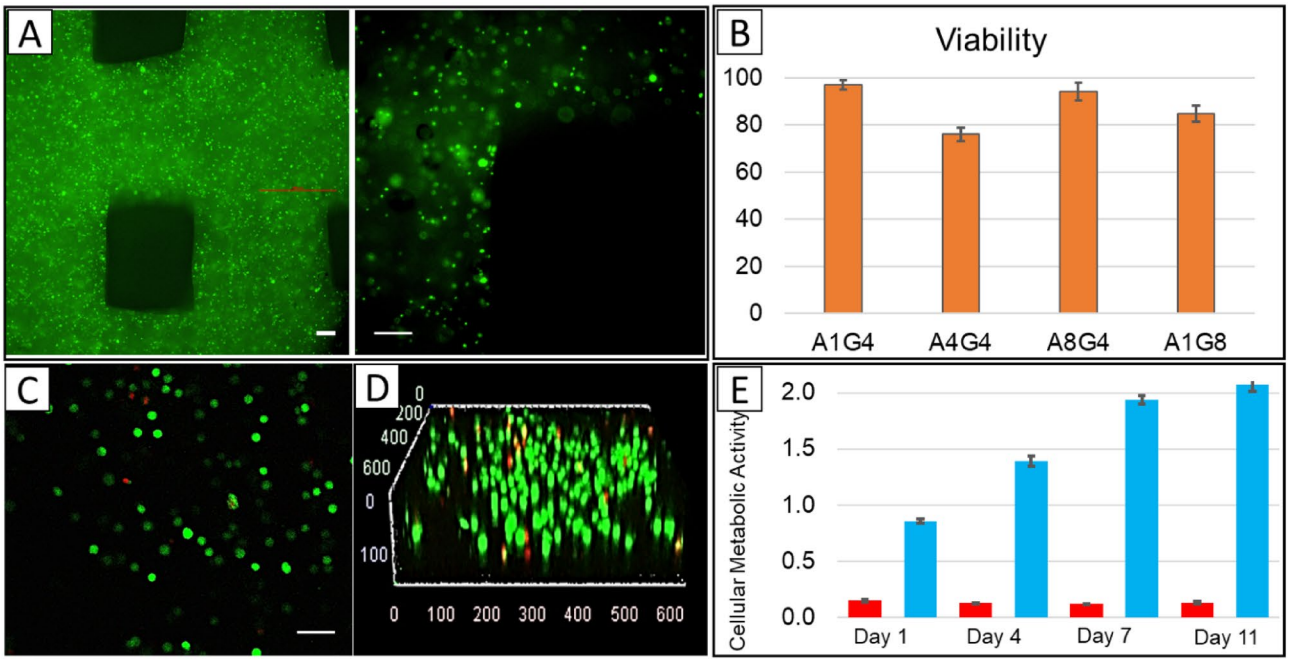

Figure 2. The uniform distribution and viability of bioprinted MDA-MD-231 cells. (**A**) Concentration and distribution of printed cells in the construct, Scale bars, 50 µm (**B**) Histogram shows the viability of the cells in the hydrogel mixtures immediately after printing. (Status of cell survival by the percentage ratio of live/dead cells). Data are expressed as the average ± standard deviation of five technical replicates of three biological replicate samples. Live-dead staining of four different hydrogel mixtures with MDA-MB-231 cells after bioprinting. (**C**) The representing image related to A4G4 with the green shows live cells and red for dead cells, Scale bar, 50 µm (**D**) 3D confocal representative image for A4G4 hydrogel. (**E**) Results of MTT assay on bioprinted constructs with A4G4 hydrogel, immediately after printing (day 1), after 4 days, after 7 days and after 11 days. Data are expressed as the average ± standard deviation of three biological replicates of samples and three biological replicates of negative controls (small bars-red colour).

the sequential bioprinted cells and bioprinted structure consisting of a mixture of both cells, respectively. In a separate experiment, the mixture of MCF7 and MDA-MB-231 cells was co-cultured in a 2D chamber. It can be seen that the cell population and the cell ratio are different at the edges of the chamber compared to the middle of the chamber, while in 3D bioprinted structure, the cells are located homogeneously (Fig. 3C–E). Although co-culturing cells in 2D conditions is also possible by seeding them over a thin layer of hydrogel to provide the proper chemical cues, the control of the precise distribution of cells would be very difficult. It should be noted that single cell cultures of MCF7 and MDA-MB-231 cells were prepared with and without cell staining to observe the effect of staining on cell growth. The co-culture with a mixture of both cells also was prepared with and without cell staining. The cell growth was observed under a microscope after 3 days and 5 days in both conditions. No noticeable differences were observed between cultures from cells with staining and without staining, which shows the staining procedure does not have an adverse effect on cell growth (data not shown here).

In order to investigate cell growth and aggregation in bioprinted co-cultures, 3D construct consisting of each cell type was separately printed and compared with the construct consisting of both cells' mixture in the bioink. A confocal microscope was used to observe the morphology of MCF7 and MDA-MB-231 cells over a 10-day experimental period in the tumor-like constructs (Fig. S2, Supporting Information). Confocal imaging of co-culture 3D bioprinted constructs shows that at day 1, both MCF7 (red) and MDA-MB-231 (green) cells are present in each layer randomly as they printed. After 3 days, both cell lines can be observed, but it seems the cells are present in different layers and migrated to make cell clusters. "It seems MCF7 cells are more likely migrate to MDA-MB-231 instead of other MCF7 cells, since more clusters of mixed cell types was observed compared to few clusters of MCF7 cells that are also observed." The cell migration inside the hydrogel is consistent with previous reports investigating the pore size of alginate-gelatin hydrogels[38,39].

Cell migration in response to chemoattractant. Here, we used epithelial growth factor (EGF), a chemoattractant material, to observe cell migration in co-cultures of the microfluidic device. The extracellular biomolecular gradients are dynamically generated within 3D hydrogel matrices via a linear gradient designed to mimic chemical environments in tumor tissues and direct cell migration. An algorithm was utilized to find the length of branches in each step of mixing channels, assuming the width of channels and their height were 400 µm and 50 µm, respectively. The whole model is 21 mm in width and 45 mm in length. Figure 4A shows the COMSOL simulation of this device in which Navier–Stokes and Convection–Diffusion equations are solved using the finite element method. In this figure, red and blue colors represent higher and lower concentrations in [mol/mm^3], respectively. The diffusion coefficient was considered to be 10^9 m^2/s which is a typical value in

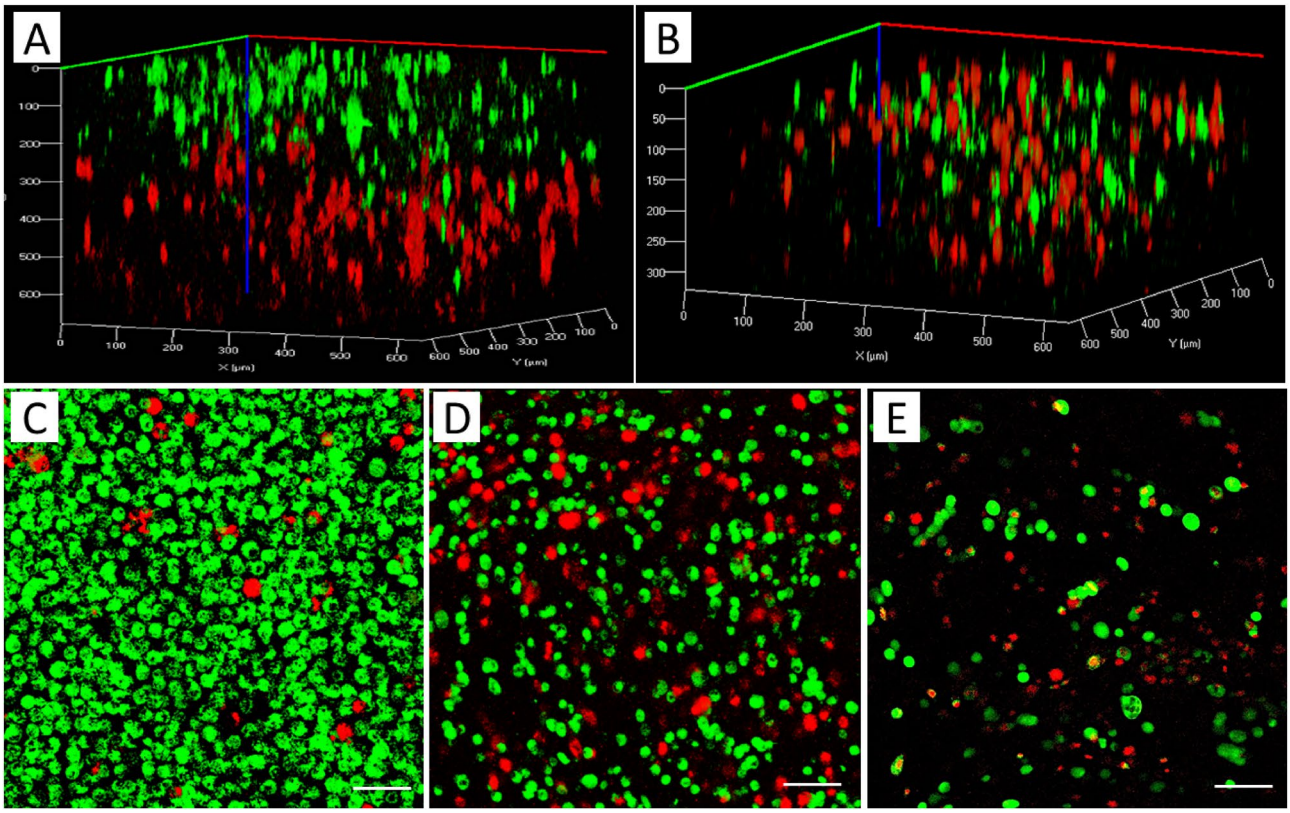

Figure 3. 3D rendered confocal images of MCF7 (stained green) and MDA-MB-231 cells (stained red): (**A**) Sequential printing of MDA-MB-231 and MCF7, (**B**) bioprinting of a construct using a bioink with a mixture of MCF7 and MDA-MB-231 cells; 2D culture of both cells mixture with the ratio of 2:1 (MCF7, green:MDA-MB-231, red): (**C**) Edge of the culture chamber, (**D**) Middle of the chamber, (**E**) 3D bioprinting of mixture cells with the ratio of 2:1 (green:red). Scale bars, 50 µm.

aqueous solutions. Pure water as the solvent and 1 [mol/mm^3] aqueous solution was supposed to enter the chip through inlets 1 and 2, respectively.

To confirm the chemical gradient, the cell culture medium and FBS were used as the source on the inlets to produce diffusion visual confirmation. Figure 4B shows the picture of the chamber with 5 min intervals applying a flow rate of 20 µl/min. The gradient has been produced and obtained for at least 5 h without the flow. The constructed co-culture of mixed MCF7 and MDA-MB-231 (Fig. 3B) were tested for migration study of two different cancer cells toward the chemoattractant (data not shown). MDA-MB-231 migration were more notable than MCF7 cells (as was expected) and we chose MDA-MB-231 for cell migration study in the next step. Our results in consistent with previous migration studies of MCF7 and MDA-MB-231 cells toward chemoattractant in microfluidic devices[40].

Bioprinted constructs, including MDA-MB-231 (labelled green) and MCF10A (labelled red) were placed in the gradient chamber. The flow rate of 5 µl/min was used with the cell culture media as the source for outlet 1 and cell culture media with 100 nM EGF as the source of outlet 2. The gradient was introduced to the cells for 8 h while the whole device was kept in 37 °C with 5% CO_2.

Figure 4C–E shows different tumor architectures of MDA-MB-231 and MCF10A cells bio-printed with ratios of MDA-MB-231 /MCF10A: 1/1 (S11), 1/4 (S14) and 4/1 (S41). The left panels show the MDA-MB-231 and MCF10A distribution in the tumor before applying EGF and the right panels shows their distribution after applying EGF. For each panel the total percentage of MDA-MB-231 cells before and after EGF exposure has been calculated and shown in the plots. The highest migration tendency observed when the ratio of cancer cells to the surrounding non-cancerous cells is 1:1 (Fig. 4C).

Discussion

Tumor heterogeneity has been observed among patients. Breast tumors are heterogeneous and consist of many different cell types that create the TME. Tumor development and the microenvironment cells have a two-way influence on each other by secreting cytokines, growth factors, etc. Besides the cancer cell-stromal cells heterogeneity, individual tumors also show heterogeneity, which was first observed about four decades ago in murine models[3] and it is named intratumor heterogeneity. Within individual cancers, there are distinct cancer cell subpopulations with variable metastatic ability due to their different representations of tumorigenicity, signaling pathways, migration, and response to anticancer drugs[5,41]. As a result, an effective model must not only provide

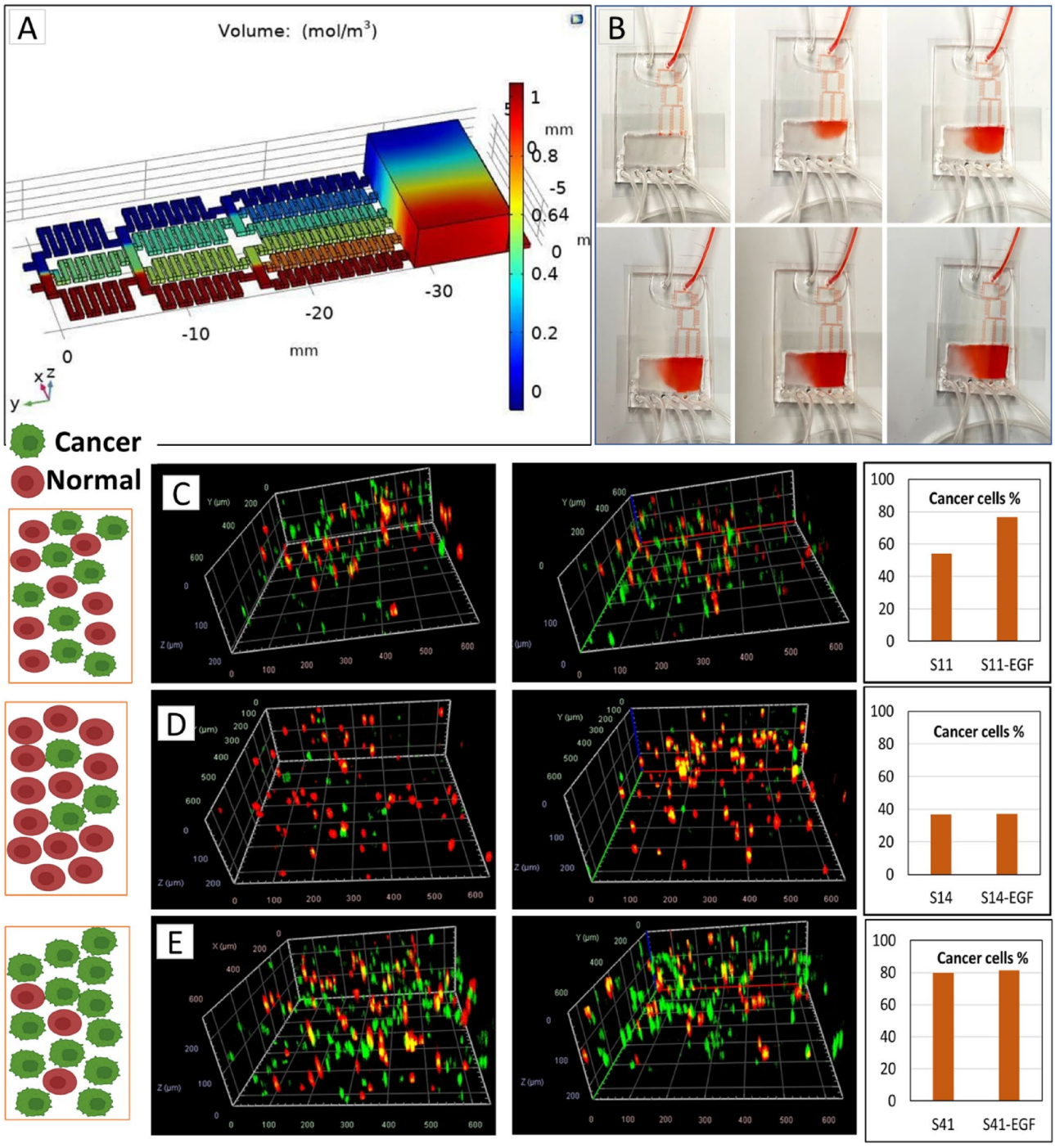

Figure 4. (**A**) COMSOL simulation of the device with red and blue represent higher and lower concentrations, (**B**) gradient formation in the 5 min intervals. The migration of MDA-MB-231 (green) and MCF10A (red) toward EGF in the microfluidic chamber; imaged on the higher concentrated of the chamber before and after EGF gradient flow: MDA-MB-231/MCF10A ratio 1:1 (S11) (**C**), MCF7/MCF10A ratio 1:4 (S14) (**D**) and MDA-MB-231/MCF10A ratio 4:1 (S41) (**E**). The respective percentage of MDA-MB-231 cells in before and after EGF exposure are shown for each panel.

a microenvironment for 3D growth of cells but also allow cell–cell interactions to study cancer progression. Any tumor-on-chip model should cover the tumor heterogeneity to be accurate.

Various 3D tissue models is created before to study two of the most important factors in cancer mortality, angiogenesis and metastasis[42]. In many metastases cases, death results from distant metastases to other organs and tissues[43,44]. Angiogenesis modeling is also a critical factor in tumor development and metastasis, allowing investigation of vascular endothelial cells' interactions with cancer cells, including the co-culture of tumor cells with endothelial cells, explanted vessels or seeded cells surrounded by tumor cell-laden hydrogels[45–47]. Here,

our goal is to establish a platform using 3D bioprinting for modeling the phenotypic heterogeneity, which is the result of different cell localization in a tumor using bio-printed tumors.

The material's intrinsic properties (including modulus, yield stress and viscosity) is the most important factor for its printability and some other external conditions are also important such as applied pressure, nozzle geometry[48]. The key component of a successful tumor 3D printing is developing an appropriate bioink. Hydrogels, with about 99% water content, are primary candidates for bioprinting since their high amount of water favors the entrapment of biological entities and increases hydrogel biocompatibility[49]. Moreover, they have significant impacts on cell proliferation, migration, aggregation, and activities that are strongly dependent to hydrogels' physical properties[50]. To date, various types of synthetic and natural polymers have been used for hydrogel preparations with different biocompatibilities and mechanical properties[50]. Polymers with low cytotoxicity and structural similarity to the ECM are good candidates for making bioinks. The primary requirements for a bioprinting material are (a) cell viability, (b) printability (shear-thinning, compatible printing pressure, continuous extrusion without air bubbles), (c) structural stability (stability of a printed structure before crosslinking and after crosslinking), and (d) rapid and non-toxic crosslinking[51].

The ideal bioink for bioprinting with extrusion methods should have relatively high viscosity, show strong shear-thinning behavior and rapidly cross link after printing. Therefore, natural polymers like alginate, gelatin, chitosan and hyaluronic acid hydrogels have attracted more attention due to their high compatibility to cell environments and good control over the quantity of ECM proteins and growth factors[51]. A widely investigated hydrogel is alginate, a natural polysaccharide derived from algae which is unique because it undergoes a sol–gel transition in the presence of divalent cations such as calcium. It also has optimal cell encapsulation properties as the slow gelation process at room temperature[52,53]. However, alginate shows poor mechanical properties. Gelatin is a highly elastic material rather than viscous and is considered to be a stiff solid bioink at room temperature[9], which is not ideal for extrusion bioprinting methods. On the other hand, if gelatin is mixed with alginate hydrogels to form a liquid phase gel, an optimum condition for bioprinting by extrusion can be achieved. Previous reports studied combinations of gelatin and alginate compatible with extrusion bioprinters[51,54]. They have also shown that gelatin provides elastic characteristics in the hydrogel, improves cell adhesion, contributes to the viscosity of the hydrogel, and adds stiffness[55,56].

A high shear stress can cause damage to the cell membrane. Therefore, the shear thinning ability is important to reduce the shear stress imparted on the cells during the extrusion process. A bioink to be considered printable should provide the opportunity for the fabrication of multi-layer porous structure without collapsing or sagging after printing. For our ink to be printable, it should exhibit sufficient yield stress to prevent its collapse, has smooth extrusion out of the nozzle such that no corrugation appears and should not show "peaks and valleys" along the extrudate or breaks within one filament.

We developed various hydrogels with alginate 1–10% and gelatin 4–10% and printed them at room temperature. By increasing the concentration of alginate from 1 to 8% while keeping the gelatin concentration about 4%, the filament quality improves, which is consistent with the report of Giuseppe[57] that increasing the concentration of alginate and gelatin resulted in more accurate printing. However, increasing the concentration of gelatin by more than 4% reduces the accuracy of the printing. It also needs higher extrusion pressure due to nozzle jamming. On the other hand, the synergetic properties of alginate-gelatin made the combination of Alginate 1%-Gelatin 8% still a good candidate for accurate printing.

Several criteria for bioink mechanical properties can be considered, but the most important one is rheology[9]. Rheology is the measurement of the deformation of a material caused by force acting on it and the vast majority of rheological characterizations of bioinks have focused on hydrogel viscosity. The rheological properties of hydrogel samples for four combinations of A1G4, A1G8, A4G4 and A8G4, (whereas A1G4 represents Alginate 1%, Gelatin 4%, etc.) with the best printability have been studied. Hydrogels with higher viscosity, experience high shear forces to extrude through the nozzle during printing. Shear thinning behavior enables highly viscous hydrogels printable with structural accuracy[58]. As it can be seen in Fig. S1C, viscosity of all hydrogels mixtures, decreased with increasing shear rate and the shear-thinning behavior was observed for all four samples. The viscosity curves of all the hydrogel mixtures showed a similar pattern, which suggests that all the hydrogels had shear thinning behavior. Based on the observation of loss and storage modulus data of hydrogels illustrated in Fig. S1D, A4G4 shows the highest storage (elastic) modulus.

The composition and mechanical properties of the hydrogel play an important role in cell viability. Based on the live-dead assay results that were previously shown in Fig. 2B, the percentage of viable MDA-MB-231 cells immediately after printing were 94.16%, 96.94%, 75.96%, and 84.7% for hydrogels A1G4, A4G4, A8G4 and, A1G8 respectively. A droplet of the A1G8 hydrogel, as a representative of not printed gel, was placed in $CaCl_2$ for crosslinking and underwent a live-dead assay process. The cell viability for A1G8 before printing was also obtained as 93.4% that is slightly higher than bioprinted one (84.7%), which is in accordance with the extrusion procedure affecting cell viability. A1G4 and A4G4 show the best cell viability results, however, A1G4 did not have a good shape fidelity in the hydrogel structure. Therefore, based on printability and viability results, A4G4 was chosen as the optimized hydrogel to be used for the co-culture experiments. Excellent viability obtained from a mixture of 4% alginate and 4% gelatin can be attributed to the soft nature of gel and cell adhesion that gelatin introduced in the hydrogel. Previous reports confirmed that when alginate concentrations are decreasing in hydrogel compositions and gelatin concentration are increasing, the gels become mechanically soft and contain a greater number of cell-adhesion moieties[59]. Our results are consistent with other reports that highly viscous hydrogels result in lower cell viability due to high extrusion pressure, which imparts higher shear stress to cells[56,60].

The MTT assay that conducted on the samples immediately after printing, and after 4, 7, and 11 days indicates the rate of viability in the 3D bioprinted constructs (Fig. 2E). The rate of viability, compared to day 1, increased over the week, which confirms the accessibility of the cells to oxygen and nutrients. The hydrogel constructs had

enough porosity and interconnected pore structure, which ensures nutrient diffusion within the construct and provides an appropriate environment for living cells. Moreover, this interconnected porous structure also allows waste product diffusion from the construct. On day 11, the absorbance was observed to be 2.07 ± 0.06, which indicates a drop in the rate of cell proliferation but shows still a very good cell viability. It seems that between day 7 to day 11 the constructs reach the maximum capacity for hosting cells and some cells started to die. These findings confirmed good biocompatibility of 3D bioprinted hydrogel constructs and showed their suitability for preserving cells viable for an extended time.

For the fabrication of co-cultures by bioprinting two different cancer cell lines, MCF7 cancer cells and MDA-MB-231 were respectively pre-stained with green and red markers before printing. The printing procedure conducted in two ways to produce two different architectures, one including two separate layers of cells and the other one randomly mixture of two cells (shown in Fig. 4A,B). It can be observed that a good control of positioning cells in the 3D construct was achieved and the cells were located homogeneously in the structure compared to the co-culture produced in 2D culture flask (Fig. 3C–E).

Tumour-on-chip models are shown more efficient models in cancer research compared to the other models, because of capability to mimic tissue-tissue interactions and tumour vascularization[61]. Developing these models is an advanced step of bioprinting and provides high-throughput testing, better microfluidic simulations, and therefore better in vitro and in vivo correlations are seen. As stated in the introduction, the metastatic spreading of a tumor begins with the acquisition of an aggressive phenotype by a subset of cells which allows them to detach from the primary tumor and migrate toward a secondary organ. Generally, breast cancer metastatic activities increase with cell–matrix interactions, mechanical stimulation and cancer cell interaction with fibroblasts and immune cells[3,62]. Therefore, for the development of metastasis activity in the designed 3D tumor, the development of a heterogeneous multicellular tumor should be considered.

Several subtypes of breast cancers were defined, with different tendencies to conduct metastases into bone[42]. In this study, we used epithelial growth factor (EGF), as a chemoattractant material and observed the cell migration in co-cultures of cancer cells, and non-tumorigenic cells using the microfluidic device. Our 3D microfluidic models have been developed to recapitulate TME heterogeneity by introducing chemical gradient, and we produce a cancer modeling platform by the combination microfluidic device and 3D bio-printing for the first time. To validate the model, triple negative malignant breast cancer cell lines (MDA-MB-231) and non-tumorigenic mammary epithelial cells (MCF10A) were embedded separately within the tumor model, all of which maintained high viability throughout the experiments (data not shown here). Then, three different tumor architectures of MDA-MB-231 and MCF10A cells bio-printed with the following ratios MDA-MB-231/MCF10A: 1/1 (S11), 1/4 (S14) and 4/1 (S41) and samples were placed in the microfluidic device chamber. The chamber was sealed, and the chemical gradient of EGF was produced for 8 h. Samples were imaged before and after applying the flow and making the EGF gradient. We compared the ratio of MDA-MB-231 cells to MCF10A cells on the top part of the scaffold which was exposed to the highest EGF concentration. MDA-MB-231 exhibited migratory behavior toward EGF and many cells were observed to move to the top of the chamber where the EGF concentration was higher (Fig. 4C–E, the second panels). However, MCF10A surrounding cells showed little net migration. The migratory behavior was different when MCF10A cells were present in the co-culture, and the ratio of cancer cells to non-cancerous cells was different. We observed the highest migration tendency when the ratio of cancer cells to the surrounding non-cancerous cells was 1:1, as shown in Fig. 4C. When the surrounding MCF10A is four times as high as the MBA-MB-231 cancer cells, the migration is negligible, and when the cancer cells are four times more populated than the surrounding cells, the migration rate is also decreased. That may be attributed to the competition of MDA-MB-231 cells toward EGF and the accumulation capacity of the scaffold.

Cell adhesion is one of the important factors in metastasis. The adhesion between tumor cells and their neighbor cells especially fibroblast was investigated in the last two decades[63,64]. It has been shown that fibroblasts can act as leader cells in metastasis by providing heterotypic mechanical adhesion to tumor cells[63,65]. It is also known that cell adhesion molecules that can act as tumor suppressors are altered in cancer thus the cancer cells may lose these surface molecules[66]. Therefore, relative number of cancer and surrounding cells and coordination of healthy and cancer cells around each other may play significant role in metastasis.

Research show that metastatic cancer occurs earlier in cancer development originating from a cell that migrates away from the breast for instance, before the primary tumor fully forms[67,68]. Our results suggest that the maximum migration happens when the number of cancer cells and non-cancerous cells in the microenvironment are similar. Therefore, when the number of cancer cells is much higher than surrounding cells, the cell mobility reduces possibility because of cancer cells higher affinity to each other. Also, the interaction between the two different cell types may prevent migration of tumor cells outwards when the surrounding healthy cells are much higher in number. This is consistent with previous reports where fibroblasts dictate the direction of migration[65]. Our architecture-based model for cancer cell migration may in the future provide significant information for prediction of time of metastasis.

Conclusion and future outlook

We successfully implemented a tumor-on-chip model based on 3D bioprinting of two different types of breast cancer cells and non-tumorigenic mammary epithelial cells. It is crucial to understand the molecular and cellular mechanisms of tumor heterogeneity for development of treatment resistance. Since breast cancer show heterogeneity both in vivo breast tumors and in vitro cell lines, investigation of tumor heterogeneity has important implications for the diagnosis, therapeutic treatment and understanding chemoresistance. Even in only one single breast tumor, different types of cancer cell populations may coexist which complicates the correct identification of the breast cancer subtypes. Furthermore, many studies show that tumor cell-cell interaction and tumor-TME interactions have significant influence on tumor progression and invasion. Our heterogeneous tumor-on-chip

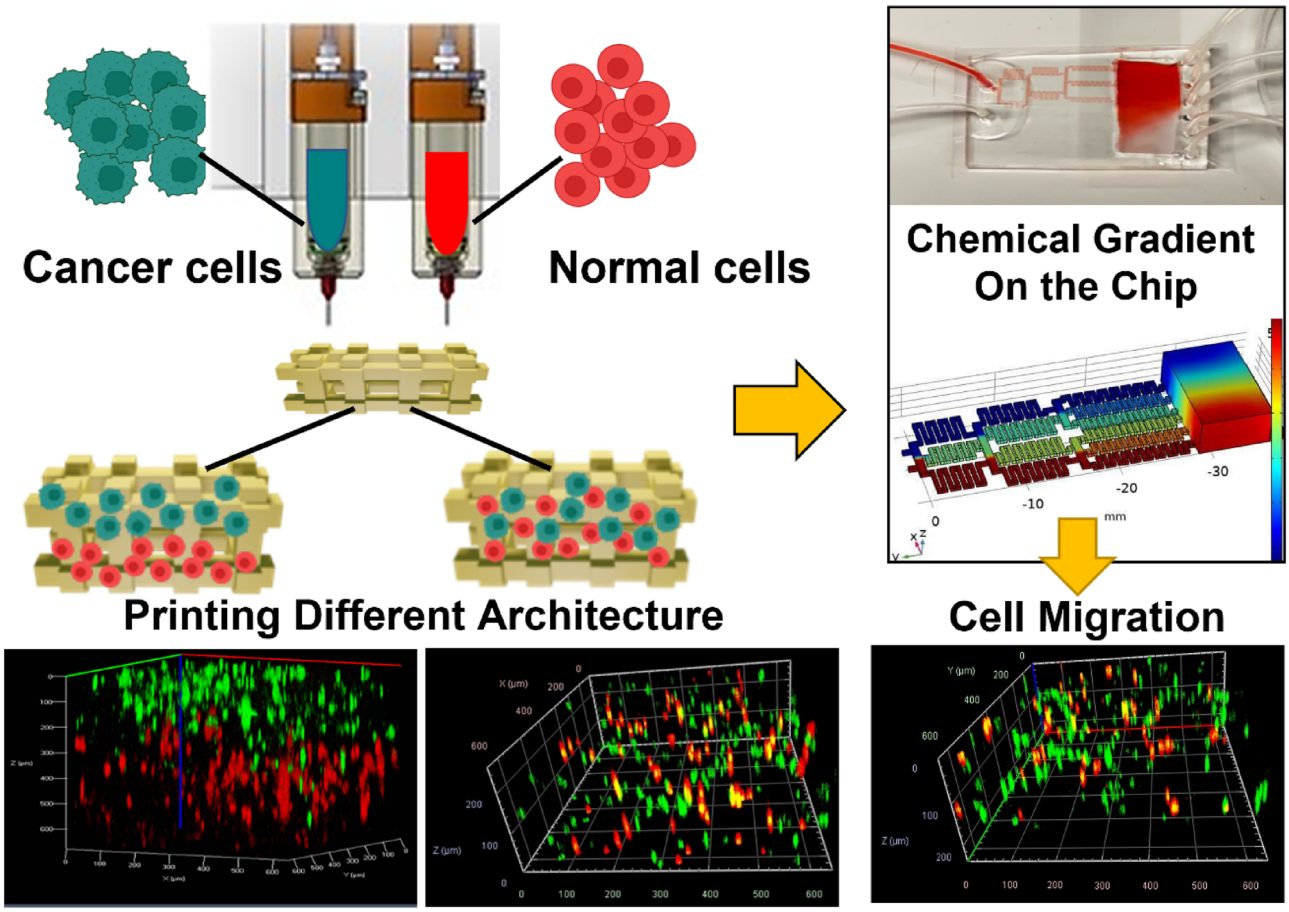

Figure 5. The summary of the proposed cancer-on-chip model.

model can have huge impact for cancer treatment research. In this study, we developed 3D bioprinting methods for building in vitro models of the TME made of different co-cultured cell types with controlled distribution and architecture in a hydrogel matrix. The tumor was represented by cancer cell/noncancerous-laden co-culture hydrogel construct, whereas its microenvironment modeled in a microfluidic chip capable of producing a chemical gradient. We investigated a composite hydrogel as a bioink, comprised of alginate and gelatin, and an optimized bioink was used for bioprinting the co-cultured constructs. The morphology and distribution of two cancer cell types, MCF7 and MDA-MB-231 were investigated by sequential bioprinting and mixed bioink bioprinting to show the accuracy of cell locations after printing. Epithelial growth factor (EGF) gradient was used as an stimulant to study cell migration in a different 3D compositional and structural format, including mixed co-culture systems of non-tumorigenic mammary epithelial cells, MCF10A and malignant MDA-MB-231 cancer cells. Figure 5, shows the summery of our proposed cancer-on-chip model.

Better understanding of the relationship between intratumor heterogeneity and tumor response to therapy will open new gateways for development of novel drugs and the use of already approved compounds in new treatment schemes or combinations for more effective personalized therapies. Our tumor-on-chip model may facilitate an understanding of cancer cell behaviour in heterogenous tumors and their microenvironment.

Data availability

All data and materials are available upon request. Please contact corresponding author nmoghimi@uwaterloo.ca.

Received: 16 May 2023; Accepted: 16 August 2023
Published online: 22 August 2023

References

1. Bray, F. *et al.* Global cancer statistics 2018: GLOBOCAN estimates of incidence and mortality worldwide for 36 cancers in 185 countries. *CA Cancer J. Clin.* **68**, 394–424 (2018).
2. Gonçalves, H. *et al.* Survival study of triple-negative and non-triple-negative breast cancer in a Brazilian cohort. *Clin. Med. Insights Oncol.* **12**, 1179554918790563 (2018).
3. Januškevičienė, I. & Petrikaitė, V. Heterogeneity of breast cancer: The importance of interaction between different tumor cell populations. *Life Sci.* **239**, 117009 (2019).
4. Visvader, J. E. Cells of origin in cancer. *Nature* **469**, 314–322 (2011).
5. Michor, F. & Polyak, K. The origins and implications of intratumor heterogeneity. *Cancer Prev. Res.* **3**, 1361–1364 (2010).
6. Bhuskute, H., Shende, P. & Prabhakar, B. 3D printed personalized medicine for cancer: Applications for betterment of diagnosis, prognosis and treatment. *AAPS PharmSciTech* https://doi.org/10.1208/s12249-021-02153-0 (2022).
7. Boix-Montesinos, P., Soriano-Teruel, P. M., Armiñán, A., Orzáez, M. & Vicent, M. J. The past, present, and future of breast cancer models for nanomedicine development. *Adv. Drug Deliv. Rev.* **173**, 306–330 (2021).
8. Moghimi, N., Hosseini, S. A., Poudineh, M. & Kohandel, M. Recent advances on cancer-on-chip models: Development of 3D tumors and tumor microenvironment. *Bioprinting* https://doi.org/10.1016/j.bprint.2022.e00238 (2022).
9. Gao, T. *et al.* Optimization of gelatin-alginate composite bioink printability using rheological parameters: A systematic approach. *Biofabrication* **10**, 1–17 (2019).
10. Yi, H. G. *et al.* A bioprinted human-glioblastoma-on-a-chip for the identification of patient-specific responses to chemoradiotherapy. *Nat. Biomed. Eng.* **3**, 509–519 (2019).
11. Meng, F. *et al.* 3D bioprinted in vitro metastatic models via reconstruction of tumor microenvironments. *Adv. Mater.* **31**, 1806899 (2019).
12. Dou, J., Mao, S., Li, H. & Lin, J. M. Combination stiffness gradient with chemical stimulation directs glioma cell migration on a microfluidic chip. *Anal. Chem.* **92**, 892–898 (2020).
13. Jeon, J. S., Zervantonakis, I. K., Chung, S., Kamm, R. D. & Charest, J. L. In vitro model of tumor cell extravasation. *PLoS ONE* **8**, e56910 (2013).
14. Jeon, J. S. *et al.* Human 3D vascularized organotypic microfluidic assays to study breast cancer cell extravasation. *Proc. Natl. Acad. Sci. U. S. A.* **112**, 214–219 (2015).
15. Vitale, C. *et al.* 3D perfusable hydrogel recapitulating the cancer dynamic environment to in vitro investigate metastatic colonization. *Polymers (Basel)* **12**, 1–19 (2020).
16. Ma, Y. *et al.* Microdroplet chain array for cell migration assays. *Lab Chip* **16**, 4658–4665 (2016).
17. Liu, Q. *et al.* Cancer cells growing on perfused 3D collagen model produced higher reactive oxygen species level and were more resistant to cisplatin compared to the 2D model. *J. Appl. Biomater. Funct. Mater.* **16**, 144–150 (2018).
18. Rodrigues, T. *et al.* Emerging tumor spheroids technologies for 3D in vitro cancer modeling. *Pharmacol. Ther.* https://doi.org/10.1016/j.pharmthera.2017.10.018 (2018).
19. Malandrino, A., Kamm, R. D. & Moeendarbary, E. In vitro modeling of mechanics in cancer metastasis. *ACS Biomater. Sci. Eng.* **4**, 294–301 (2018).
20. Augustine, R. *et al.* Gelatin-methacryloyl hydrogel based in vitro blood–brain barrier model for studying breast cancer-associated brain metastasis. *Pharm. Dev. Technol.* **26**, 490–500 (2021).
21. Derby, B. Printing and prototyping of tissues and scaffolds. *Science (1979)* **338**, 921 (2012).
22. Knowlton, S., Onal, S., Yu, C. H., Zhao, J. J. & Tasoglu, S. Bioprinting for cancer research. *Trends Biotechnol.* **33**, 504–513 (2015).
23. Bojin, F. *et al.* 3D bioprinting of model tissues that mimic the tumor microenvironment. *Micromachines (Basel)* **12**, 1–17 (2021).
24. Datta, P., Dey, M., Ataie, Z., Unutmaz, D. & Ozbolat, I. T. 3D bioprinting for reconstituting the cancer microenvironment. *NPJ Precis. Oncol.* **4**, 18 (2020).
25. Kang, Y., Datta, P., Shanmughapriya, S. & Ozbolat, I. T. 3D bioprinting of tumor models for cancer research. *ACS Appl. Bio Mater.* **3**, 5552–5573 (2020).
26. Murphy, S. V. & Atala, A. 3D bioprinting of tissues and organs. *Nat. Biotechnol.* **32**, 773–785 (2014).
27. Hull, S. M., Brunel, L. G. & Heilshorn, S. C. 3D bioprinting of cell-laden hydrogels for improved biological functionality. *Adv. Mater.* https://doi.org/10.1002/adma.202103691 (2021).
28. Kang, H. W. *et al.* A 3D bioprinting system to produce human-scale tissue constructs with structural integrity. *Nat. Biotechnol.* **34**, 312–319 (2016).
29. Jia, W. *et al.* Direct 3D bioprinting of perfusable vascular constructs using a blend bioink. *Biomaterials* **106**, 58–68 (2016).
30. Miller, J. S. *et al.* Rapid casting of patterned vascular networks for perfusable engineered three-dimensional tissues. *Nat. Mater.* **11**, 768–774 (2012).
31. Lee, V. *et al.* Design and fabrication of human skin by three-dimensional bioprinting. *Tissue Eng. Part C Methods* **20**, 473–484 (2014).
32. Li, J. *et al.* Engineering functional skin constructs: A quantitative comparison of three-dimensional bioprinting with traditional methods. *Exp. Dermatol.* https://doi.org/10.1111/exd.14488 (2021).
33. Sala, F., Ficorella, C., Osellame, R., Käs, J. A. & Martínez Vázquez, R. Microfluidic lab-on-a-chip for studies of cell migration under spatial confinement. *Biosensors (Basel)* **12**, 604 (2022).
34. Kalot, R., Mhanna, R. & Talhouk, R. Organ-on-a-chip platforms as novel advancements for studying heterogeneity, metastasis, and drug efficacy in breast cancer. *Pharmacol. Ther.* https://doi.org/10.1016/j.pharmthera.2022.108156 (2022).
35. Ouyang, L., Yao, R., Zhao, Y. & Sun, W. Effect of bioink properties on printability and cell viability for 3D bioplotting of embryonic stem cells. *Biofabrication* **8**, 035020 (2016).
36. Wallace, P. K. *et al.* Tracking antigen-driven responses by flow cytometry: Monitoring proliferation by dye dilution. *Cytometry A* **73**, 1019–1034 (2008).
37. Nair, K. *et al.* Characterization of cell viability during bioprinting processes. *Biotechnol. J.* **4**, 1168–1177 (2009).
38. Hwang, C. M. *et al.* Fabrication of three-dimensional porous cell-laden hydrogel for tissue engineering. *Biofabrication* **2**, 035003 (2010).
39. Chen, Q. *et al.* An interpenetrating alginate/gelatin network for three-dimensional (3D) cell cultures and organ bioprinting. *Molecules* **25**, 756 (2020).
40. Poudineh, M. *et al.* Profiling functional and biochemical phenotypes of circulating tumor cells using a two-dimensional sorting device. *Angew. Chem.* **129**, 169–174 (2017).
41. Andrechek, E. R. & Nevins, J. R. Mouse models of cancers: Opportunities to address heterogeneity of human cancer and evaluate therapeutic strategies. *J. Mol. Med.* **88**, 1095–1100 (2010).
42. Arrigoni, C., Bersini, S., Gilardi, M. & Moretti, M. In vitro co-culture models of breast cancer metastatic progression towards bone. *Int. J. Mol. Sci.* **17**, 1405 (2016).
43. Weigelt, B., Peterse, J. L. & Van't Veer, L. J. Breast cancer metastasis: Markers and models. *Nat. Rev. Cancer* **5**, 591–602 (2005).
44. Coleman, R. E. & Rubens, R. D. The clinical course of bone metastases from breast cancer. *Br. J. Cancer* **55**, 61–66 (1987).
45. Swaminathan, S., Hamid, Q., Sun, W. & Clyne, A. M. Bioprinting of 3D breast epithelial spheroids for human cancer models. *Biofabrication* **11**, 025003 (2019).

46. Phamduy, T. B. *et al.* Printing cancer cells into intact microvascular networks: A model for investigating cancer cell dynamics during angiogenesis. *Integr. Biol. (United Kingdom)* **7**, 1068–1078 (2015).
47. Seano, G. *et al.* Modeling human tumor angiogenesis in a three-dimensional culture system. *Blood* **121**, e129–e137 (2013).
48. Naghieh, S. & Chen, X. Printability—A key issue in extrusion-based bioprinting. *J. Pharm. Anal.* **11**, 564–579 (2021).
49. Grijalvo, S., Nieto-Díaz, M., Maza, R. M., Eritja, R. & Díaz, D. D. Alginate hydrogels as scaffolds and delivery systems to repair the damaged spinal cord. *Biotechnol. J.* **14**, 1900275 (2019).
50. Amekyeh, H., Tarlochan, F. & Billa, N. Practicality of 3D printed personalized medicines in therapeutics. *Front. Pharmacol.* **12**, 1–15 (2021).
51. Mondal, A. *et al.* Characterization and printability of Sodium alginate-Gelatin hydrogel for bioprinting NSCLC co-culture. *Sci. Rep.* **9**, 1–12 (2019).
52. Bendtsen, S. T., Quinnell, S. P. & Wei, M. Development of a novel alginate-polyvinyl alcohol-hydroxyapatite hydrogel for 3D bioprinting bone tissue engineered scaffolds. *J. Biomed. Mater. Res. A* **105**, 1457–1468 (2017).
53. Luo, Y., Lode, A., Sonntag, F., Nies, B. & Gelinsky, M. Well-ordered biphasic calcium phosphate-alginate scaffolds fabricated by multi-channel 3D plotting under mild conditions. *J Mater Chem B* **1**, 4088–4098 (2013).
54. Pan, T., Song, W., Cao, X. & Wang, Y. 3D bioplotting of gelatin/alginate scaffolds for tissue engineering: Influence of crosslinking degree and pore architecture on physicochemical properties. *J. Mater. Sci. Technol.* **32**, 889–900 (2016).
55. Wang, X. *et al.* Gelatin-based hydrogels for organ 3D bioprinting. *Polymers (Basel)* **9**, 401 (2017).
56. Zhao, Y., Li, Y., Mao, S., Sun, W. & Yao, R. The influence of printing parameters on cell survival rate and printability in microextrusion-based 3D cell printing technology. *Biofabrication* **7**, 045002 (2015).
57. Di Giuseppe, M. *et al.* Mechanical behaviour of alginate-gelatin hydrogels for 3D bioprinting. *J. Mech. Behav. Biomed. Mater.* **79**, 150–157 (2018).
58. Panwar, A. & Tan, L. P. Current status of bioinks for micro-extrusion-based 3D bioprinting. *Molecules* **21**, 685 (2016).
59. Jiang, T. *et al.* Engineering bioprintable alginate/gelatin composite hydrogels with tunable mechanical and cell adhesive properties to modulate tumor spheroid growth kinetics. *Biofabrication* **12**, 015024 (2020).
60. Jang, J., Park, J. Y., Gao, G. & Cho, D. W. Biomaterials-based 3D cell printing for next-generation therapeutics and diagnostics. *Biomaterials* **156**, 88–106 (2018).
61. Bishop, E. S. *et al.* 3-D bioprinting technologies in tissue engineering and regenerative medicine: Current and future trends. *Genes Dis.* **4**, 185–195 (2017).
62. Sharifi, M. *et al.* 3D bioprinting of engineered breast cancer constructs for personalized and targeted cancer therapy. *J. Control. Release* **333**, 91–106 (2021).
63. Urdal, J., Waldeland, J. O. & Evje, S. Enhanced cancer cell invasion caused by fibroblasts when fluid flow is present. *Biomech. Model Mechanobiol.* **18**, 1047–1078 (2019).
64. Shieh, A. C., Rozansky, H. A., Hinz, B. & Swartz, M. A. Tumor cell invasion is promoted by interstitial flow-induced matrix priming by stromal fibroblasts. *Cancer Res.* **71**, 790–800 (2011).
65. Waldeland, J. O., Polacheck, W. J. & Evje, S. Collective tumor cell migration in the presence of fibroblasts. *Biomechanic* **18**, 1047–1078 (2012).
66. Moh, M. C. & Shen, S. The roles of cell adhesion molecules in tumor suppression and cell migration A new paradox. *Cell Adhes. Migr.* **3**, 334–336 (2009).
67. Whately, K. M. *et al.* Nuclear Aurora-A kinase-induced hypoxia signaling drives early dissemination and metastasis in breast cancer: Implications for detection of metastatic tumors. *Oncogene* **40**, 5651–5664 (2021).
68. Patras, L., Paul, D. & Matei, I. Weaving the nest: Extracellular matrix roles in pre-metastatic niche formation. *Front. Oncol.* **13**, 1163786 (2023).

Author contributions

N.M. designed the experiments, analyzed data, and wrote the manuscript. S.A.H. designed the microfluidic device and relevant simulations. D.M. helped in cell culture experiments. A.B.D. helped in cell culture experiments, data analysis and interpretation of the experimental results. A.G. and M.K. supervised the research. All authors read and approved the final manuscript. All authors read the manuscript and agreed to publish it in Biomaterials Research.

Funding

The financial support from the Canadian Institutes of Health Research (CIHR) (***) is gratefully acknowledged.

Competing interests

The authors declare that they have no known competing financial interests or personal relationships that could have appeared to influence the work reported in this paper.

Additional information

Supplementary Information The online version contains supplementary material available at https://doi.org/10.1038/s41598-023-40680-x.

Correspondence and requests for materials should be addressed to N.M.